RSC Advances

PAPER

View Article Online
View Journal | View Issue

Cite this: *RSC Adv.*, 2017, **7**, 53604

Facile synthesis of a dopant-free hole transporting material with a phenothiazine core for planar perovskite solar cells†

Xiaoyuan Liu,[ab] Xiao Tan,[a] Qian Chen,[b] Haiquan Shan,[b] Changmei Liu,[a] Jiaju Xu,[b] Zhi-Kuan Chen,*[a] Wei Huang*[a] and Zong-Xiang Xu *[b]

Received 27th September 2017
Accepted 13th November 2017

DOI: 10.1039/c7ra10677g

rsc.li/rsc-advances

A novel electron-rich small-molecule, 4,4′-(10-(4-octylphenyl)-10*H*-phenothiazine-3,7-diyl)bis(*N*,*N*-(4-methoxyphenyl)anilene) (PTZ-TPA), containing phenothiazine as the core with triphenylamine side groups, was synthesized *via* a Suzuki–Miyaura cross-coupling reaction. When PTZ-TPA was incorporated into a $CH_3NH_3PbI_3$ perovskite solar cell as a dopant-free hole transporting material (HTM), a short circuit photocurrent density of 21.5 mA cm^{-2}, an open circuit voltage of 0.982 V, and a fill factor of 0.679 were obtained, giving rise to an overall power conversion efficiency of 14.3%, which is comparable to the power conversion efficiency obtained using the current state-of-the-art HTM 2,20,7,70-tetrakis(*N*,*N*′-di-*p*-methoxyphenylamine)-9,90-spirobifluorene with dopant (Spiro-MeOTAD, power conversion efficiency of 17.1%). PTZ-TPA is thus a promising HTM with the potential to replace the expensive Spiro-MeOTAD owing to its comparable performance and much simpler synthesis route; it also presented a better stability during a one week aging test compared with Spiro-MeOTAD.

1. Introduction

In the past few years, organic–inorganic metal halide perovskite solar cells (PSCs) have emerged as a competitive alternative to conventional inorganic solar cells, owing to the ease of their fabrication processes, relatively cheap materials, and very high power conversion efficiencies.[1–4] Perovskite light absorbers possess several appealing optoelectronic properties, such as a broad spectral absorption range, high absorption coefficient, low exciton binding energy, high charge carrier mobility, and long carrier diffusion length. Significant progress has been made in PSCs over the past few years and the power conversion efficiency (PCE) of PSCs has increased dramatically from an initial value of 3.8% (ref. 5) to a certified value of 22.1% in 2016.[6]

In the most efficient PSC devices with a regular n–i–p cell configuration, hole-transporting materials (HTMs) are indispensable for achieving high PCEs.[7,8] They play an important role in extracting photo-generated holes from the perovskite layer and transporting them to the cathode, thereby circumventing undesired recombination losses at the interfaces. Numerous small organic molecules have been investigated as HTMs in PSCs. To date, the highest reported PCEs have been reached with molecules such as 2,20,7,70-tetrakis(*N*,*N*′-di-*p*-methoxyphenylamine)-9,90-spirobifluorene (Spiro-MeOTAD) that have the spiro functionality as a common structural feature. However, Spiro-MeOTAD suffers from a low hole mobility and low conductivity in its pristine form because of its amorphous nature. Thus p-type dopants or additives such as lithium bis(trifluoromethanesulfonyl)imide (Li-TFSI) are ubiquitously adopted to generate free carriers and to increase conductivity for higher efficiencies.[9,10] However, the introduction of p-type dopants not only complicates the optimization process, but also induces additional production costs. Moreover, lithium salts are hydroscopic, which may accelerate the degradation of PSC devices.[9] In this regard, a great deal of research efforts have been devoted to developing dopant-free HTMs for PSCs; alternative building blocks, such as fluorene,[11,12] dithienosilole,[13] diketopyrrolopyrrole,[14] triphenylamine,[11,15,16] benzodithiophene,[17] tetraphenylethene,[18] C3h truxene,[19] bithiophene,[20] indacenodithienothiophene,[21] and copper(II) phthalocyanine,[22] have been used for the molecular cores to reach state-of-the-art photovoltaic figures of merit in PSCs. To further improve the stability of PSCs and enrich our understanding of the relationship between HTM structures and PSC performance, we must extend the scope of our search for HTMs.

Phenothiazine derivatives have a well-conjugated heterocyclic ring system and they are widely used in dye sensitized solar cells and organic solar cells;[23,24] phenothiazine derivatives

[a]*Key Laboratory of Flexible Electronics (KLOFE), Institute of Advanced Materials (IAM), National Jiangsu Synergetic Innovation Center for Advanced Materials, Nanjing Tech University, 30 South Puzhu Road, Nanjing 211816, P. R. China. E-mail: iamzkchen@njtech.edu.cn; iamwhuang@njtech.edu.cn*

[b]*Department of Chemistry, South University of Science and Technology of China, Shenzhen, P. R. China. E-mail: xu.zx@sustc.edu.cn*

† Electronic supplementary information (ESI) available. See DOI: 10.1039/c7ra10677g

possess unique electronic and optical properties. Further, there has also been a report on a doped HTM incorporating phenoxazine;[25] this system has been proven to be effective as a HTM in PSCs. These reports demonstrate that the minor structural difference between PTZ1 and PTZ2 dramatically influence the molecular geometry and relevant optoelectronic parameters for HTMs in perovskite solar cells. These studies did, however, reveal the potential versatility of the phenothiazine building block for the development of inexpensive and efficient molecular HTMs for perovskite-based solar cells. Our previous work showed that the use of an alkyl chain results in a higher hydrophobicity, which can prevent the penetration of atmospheric moisture into the perovskite layer. This may improve device stability.[26]

The present study reports a novel 4,4′-(10-(4-octylphenyl)-10*H*-phenothiazine-3,7-diyl)bis(*N*,*N*-(4-methoxyphenyl)anilene) (PTZ-TPA) material (Scheme 1) based on an electron-rich phenothiazine core. Phenothiazine is a low-cost and flexible electron-rich heteroaromatic unit, which provides access to a wide library of HTMs with relatively cheap synthetic procedures.[27] In this work, an electron rich phenothiazine was used as the core to which hole accepting triphenylamine moieties were linked, while hexyl chains were attached to the core's carbon atom to increase the molecule's solubility and hydrophobicity.[28] The phenothiazine core has a planar structure relative to triphenylamine, which is desirable for promoting intramolecular π-delocalization and intermolecular π–π stacking, which increases both the charge carrier mobility and the lifetime, thus boosting device efficiency.[29] PTZ-TPA was synthesized from a relatively inexpensive commercially available phenothiazine derivative in a single step with an acceptable yield (79%). In addition to an extensive investigation of its material properties, we have also investigated the performance of PTZ-TPA in planar perovskite solar cells in terms of their *J*–*V* characteristics and charge carrier dynamics. The devices fabricated using dopant free PTZ-TPA demonstrated a PCE of 14.3%, which is comparable to the values obtained using state-of-the-art Spiro-MeOTAD with a dopant; additionally, our fabricated devices showed a better device stability.

2. Experimental sections

2.1 Materials and instruments

All materials were used as purchased without further purification unless specified otherwise. Organic solvents were purchased from Sigma Aldrich. Spiro-MeOTAD, CH_3NH_3I, and PbI_2 were purchased from TCI.

PTZ-TPA was synthesized using a one-step Suzuki–Miyaura cross-coupling reaction. A mixture of 4-methoxy-*N*-(4-methoxyphenyl)-*N*-(4-(4,4,5,5-tetramethyl-1,3,2-dioxaborolan-2-yl)phenyl) aniline (0.560 g, 2.20 mmol), 3,7-dibromo-10-(4-octylphenyl)-10*H*-phenothiazine (0.545 g, 1.00 mmol), and $Pd(PPh_3)_4$ (0.028 g, 0.025 mmol) in toluene (10 mL) and a 2 M K_2CO_3 aqueous solution (5 mL) was stirred at 100 °C for 24 h. After cooling down the reaction mixture to room temperature, the mixture was diluted with dichloromethane and washed with water. The organic layer was dried over Na_2SO_4 and the remaining solvent was evaporated. The crude product was purified by column chromatography (SiO_2, petroleum ether/CH_2Cl_2 = 1/4 vol/vol) to obtain PTZ-TPA (0.789 g, 79.3% yield) as a yellow solid (^{1}H NMR (500 MHz, CD_2Cl_2) δ 7.95–6.10 (34H, m), 3.78 (12H, s), 2.73 (2H, s), 1.71 (2H, s), 1.30 (11H, s), 0.89 (3H, s); MS: *m*/*z* (M^+) 992.544).

The ultraviolet-visible (UV-vis) spectra of the solutions and of the solid thin films were obtained on a PerkinElmer Lambda750S spectrophotometer. Thermogravimetric analysis (TGA) was performed using a Discovery thermogravimetric analyzer. ^{1}H NMR spectroscopy was performed using a Bruker DPX 400 MHz spectrometer. Matrix assisted laser desorption/ionization time-of-flight mass spectra were obtained on a Bruker Daltonics flexAnalysis. The highest occupied molecular orbital (HOMO) energy level of PTZ-TPA was measured using photoelectron yield spectroscopy under N_2 (Model IPS-4). Steady-state photoluminescence spectra were measured using a FLS980 Spectrometer (Edinburgh Instruments). The samples were excited through the perovskite or PTZ-TPA layer with an excitation wavelength of 475 nm. Room-temperature photoluminescence (PL) decay curves were acquired for the perovskite films on fluorine doped tin oxide (FTO), for the perovskite films on PCBM/SnO_2/FTO, of the Spiro-MeOTAD device, and of the PTZ-TPA/perovskite/PCBM/SnO_2/FTO stack (excitation using a 405 nm-wavelength pulsed laser). The hole mobilities of PTZ-

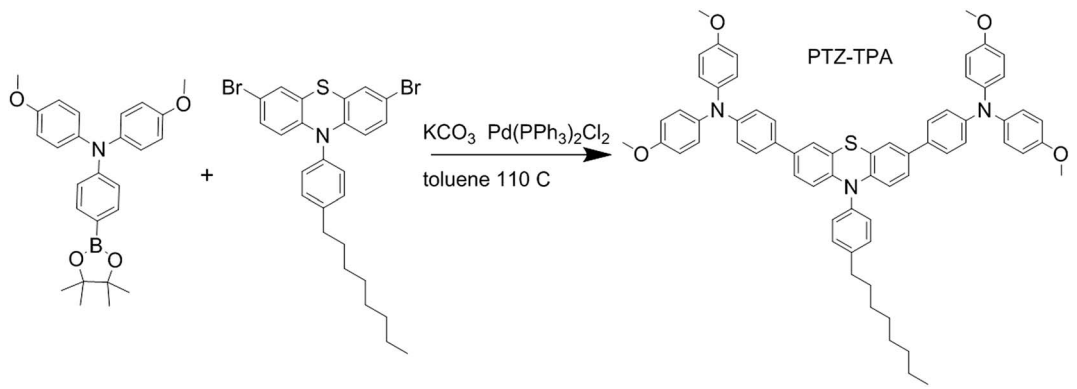

Scheme 1 Synthesis route of PTZ-TPA.

TPA and Spiro-MeOTAD were estimated using the space-charge limited current method with devices with a structure consisting of ITO/PEDOT:PSS/PTZ-TPA or Spiro-MeOTAD/Au. The current *J–V* curves of the devices were recorded using a Keithley 2400 source. Hole mobilities were calculated using the Mott–Gurney law by fitting eqn (1), where J is the current density, ε_0 is the permittivity of free space (8.85×10^{-12} F m^{-1}), ε is the relative permittivity of the material (approaching 3 for organic semiconductors), μ is the hole mobility, V is the applied voltage, and d is the thickness of the active layer, respectively.

$$J = \frac{9}{8}\varepsilon\varepsilon_0\mu\frac{V^2}{d^3} \quad (1)$$

2.2 Device fabrication

PSCs were fabricated with the following structure: FTO/SnO_2/PCBM/perovskite/PTZ-TPA/Au on patterned FTO glass. The FTO glass (with a sheet resistance of 20 Ω $\square^{-1}$, PV Tech, China) substrates were pre-cleaned using an ultrasonic bath of chlorobenzene and acetone followed by a treatment in an ultraviolet-ozone chamber (Novascan Company, USA) for 15 min. The SnO_2 electron transport layer was applied following a previously reported procedure.[30] $SnCl_2 \cdot 2H_2O$ in ethanol was used as a precursor solution (0.1 M). The precursor solution was spin-coated onto the substrate at a speed of 3000 rpm for 30 s and then the films were annealed under an ambient atmosphere at 180 °C for 1 h. A thin layer of PCBM (10 nm) was prepared on the FTO/SnO_2 surface at a speed of 2000 rpm and annealed at 100 °C for 10 min. The PCBM solutions were prepared by dissolving 15 mg PCBM in 1 mL chlorobenzene. The perovskite ($CH_3NH_3PbI_3$) layer (~320 nm) was then fabricated on the SnO_2 film. The film was annealed at 90 °C for 15 min. The hole-transporting materials PTZ-TPA (41 nm) were deposited by spin coating at 4000 rpm for 30 s from a chlorobenzene solution. The thickness of the photosensitive layer was measured using an Ambios Technology (USA) XP-2 profilometer. Finally, a 100 nm-thick Au film was deposited by thermal evaporation (Mbraun MB200) as the cathode. The active area (0.11 cm^2) of the devices was determined by the overlap of FTO and the gold electrode. The current density–voltage (*J–V*) characteristics of the devices were measured with a computer-controlled Keithley (Zolix ss150 Solar Simulator) 236 source meter. The light source was a xenon lamp coupled with an AM1.5 solar spectrum filter; the optical power at the sample was 100 mW cm^{-2}. The incident photon-to-current conversion efficiency (IPCE) spectra were recorded using a solar cell quantum efficiency/external quantum efficiency measurement system (Zolix Solar cell scan 100) model SR830 DSP lock-in amplifier coupled with a WDG3 monochromator and a 500 W xenon lamp.

3. Results and discussion

All materials were purchased from Sigma Aldrich and used as received. The synthesis route of PTZ-TPA (Scheme 1) is shorter and less expensive compared with that of Spiro-MeOTAD. The commercially available relatively inexpensive material 3,7-dibromo-10-(4-octylphenyl)-10*H*-phenothiazine was Suzuki coupled with a triphenylamine derivative[31] to give PTZ-TPA in a 79% yield from an unoptimised reaction. NMR spectroscopy and matrix assisted laser desorption/ionization time-of-flight mass spectrometry confirmed the molecular structure of PTZ-TPA (Fig. S1 and S2 ESI†). The thermal gravimetric analysis of PTZ-TPA is shown in Fig. S3 (ESI†). A decomposition temperature (5% weight loss) of 464 °C was observed for PTZ-TPA. The material exhibited an excellent thermal stability. Fig. S4 (ESI†) shows the chemical structure of the PTZ-TPA and Spiro-MeOTAD together with the electronic density distribution of their frontier orbitals as calculated by density functional theory. For PTZ-TPA, the HOMO level shows a π-bonding character, spreading over the whole molecule, while the lowest unoccupied molecular orbital (LUMO) shows a π*-antibonding character, as it is predominately localized on the central phenothiazine unit and on the two benzene units. The calculated HOMO energy of PTZ-TPA (−4.45 eV) is relatively close to that of Spiro-MeOTAD (−4.31 eV), which should promote effective hole transfer from the perovskite layer to PTZ-TPA.[32]

Table 1 summarizes the optical and electrochemical properties of the two HTMs. The optoelectronic properties of PTZ-TPA have been systematically investigated and compared with those of Spiro-MeOTAD. In the UV-vis absorption spectra (shown in Fig. 1a), the absorption peaks of PTZ-TPA and Spiro-MeOTAD can be observed at 338 and 374 nm, respectively. The absorption onset wavelengths of PTZ-TPA and Spiro-MeOTAD are at 459 and 420 nm, respectively, which corresponds to band gaps of 2.70 and 2.95 eV, respectively. The onset of absorption in PTZ-TPA was slightly red shifted with respect to that in Spiro-MeOTAD, which can be attributed to the more extended conjugation in the backbone of PTZ-TPA because of the presence of two extra phenyl rings between the nitrogen atoms. Obtained from the ionization energy measurement system of PTZ-TPA and Spiro-MeOTAD, the HOMO levels of PTZ-TPA and Spiro-MeOTAD are 5.21 and 5.11 eV, respectively,

Table 1 Optical and electrochemical properties of PTZ-TPA and Spiro-MeOTAD

Compounds	λ_{maxsol} (nm)	$\lambda_{maxfilm}$ (nm)	λ_{onset} (nm)	HOMO[a] (eV)	LUMO[b] (eV)	Band gap[c] (eV)
PTZ-TPA	329	338	459	−5.21	−2.51	2.70
Spiro-MeOTAD	385	374	420	−5.11	−2.16	2.95

[a] HOMO energy level was measured by photoelectron yield spectroscopy. [b] LUMO calculated by LUMO = HOMO + band gap. [c] Optical band gap obtained from the onset value of absorption (λ_{onset}).

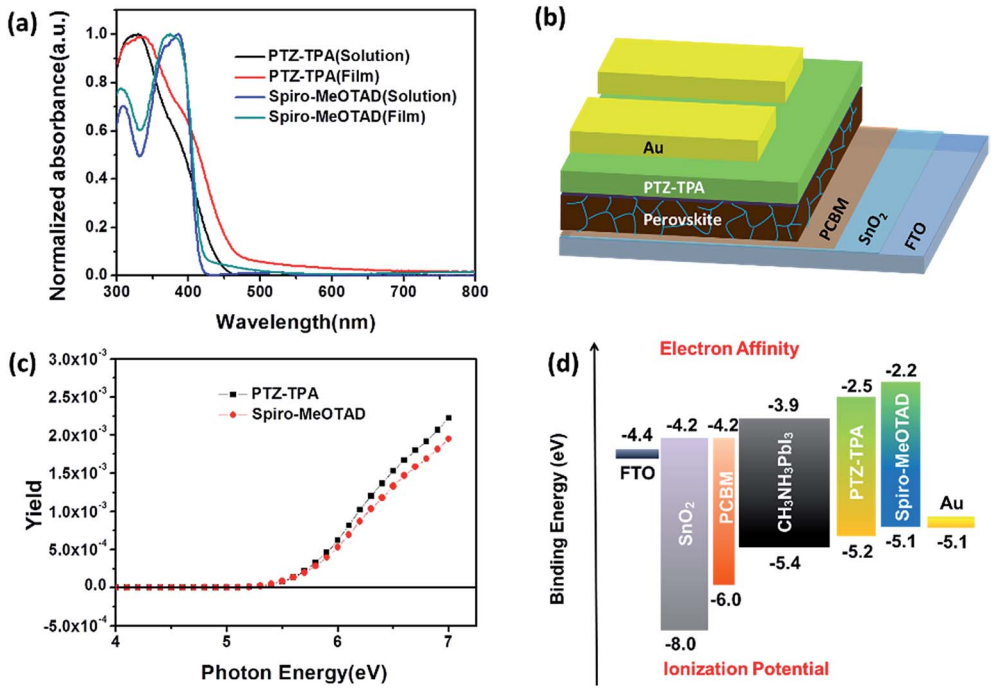

Fig. 1 (a) UV-vis absorption spectra of PTZ-TPA and Spiro-MeOTAD in a CH_2Cl_2 solution and as thin films on a glass substrate. (b) Schematic device architecture of the PSCs studied. (c) The HOMO energy level of PTZ-TPA as measured by photoelectron yield spectroscopy (under N_2). (d) Energy level diagram of the various components of the PSCs.

while the reported HOMO energy level of $CH_3NH_3PbI_3$ is 5.40 eV, which indicates that PTZ-TPA has favourable energetics for hole transfer (Fig. 1c). And the results are given in Table 1 and shown in Fig. 1c. The energetics of the system employing PTZ-TPA/Spiro-MeOTAD are presented in Fig. 1d.

Hole mobility is an important parameter for HTMs. The hole mobilities of PTZ-TPA and Spiro-MeOTAD were estimated using the space-charge limited current method with devices with a structure consisting of indium tin oxide/PEDOT:PSS/PTZ-TPA or Spiro-MeOTAD/Au (Fig. S5†). The extracted hole mobility of the undoped PTZ-TPA was 6.75×10^{-4} cm^2 V^{-1} s^{-1}, which is considerably higher than that of Spiro-MeOTAD (1.06×10^{-5} cm^2 V^{-1} s^{-1}). Therefore, it is a realistic hypothesis that a better photovoltaic performance should be obtained using PTZ-TPA as a HTM in a PSC; such a PSC was thus fabricated and the results discussed in detail later in this report.

We investigated the photovoltaic properties of PTZ-TPA and Spiro-MeOTAD as HTMs in PSCs. The optimized device structure ($FTO/SnO_2/PC_{61}BM/CH_3NH_3PbI_3/HTMs/Au$) is shown in Fig. 1b. The devices were prepared according to protocols reported in the literature.[22]

The photovoltaic performances of PSCs employing dopant-free PTZ-TPA as a HTM were measured under AM 1.5G (100 mW cm^{-2}) simulated light illumination. For comparison, a reference cell with Spiro-MeOTAD with and without a Li-TFSI dopant and a 4-*tert*-butylpyridine (*t*-BP) additive was also fabricated under similar conditions. The current density–voltage (*J*–*V*) characteristics of the perovskite solar cells are

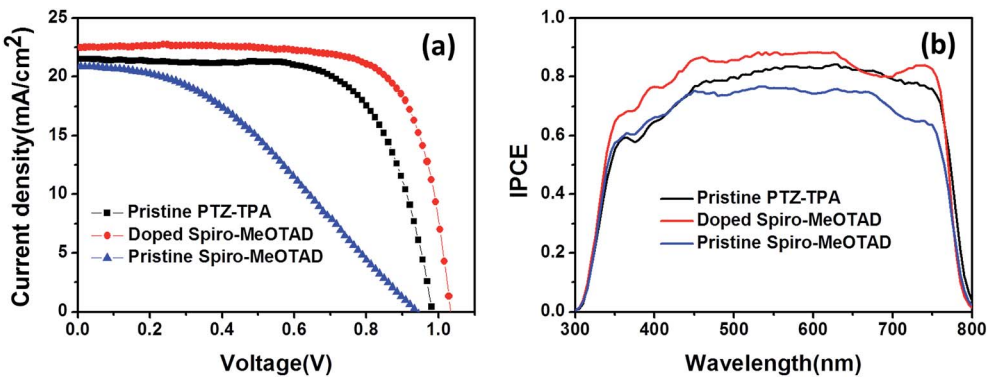

Fig. 2 (a) *J*–*V* characteristics of the PSC devices studied. (b) IPCE spectra of PSC devices with pristine PTZ-TPA, pristine Spiro-MeOTAD, and doped Spiro-MeOTAD as a HTM.

Table 2 J–V characteristics of PSCs based on different HTMs measured under 100 mW cm^{-2} illumination (AM 1.5G)

HTMs	J_{sc} (mA cm^{-2})	V_{oc} (V)	FF (%)	PCE (%)
Doped Spiro-MeOTAD	22.5	1.03	73.7	17.1
Pristine Spiro-MeOTAD	20.9	0.939	37.6	7.39
Pristine PTZ-TPA[a]	21.5 (21.5 ± 0.57)	0.982 (0.959 ± 0.022)	67.9 (65.2 ± 1.9)	14.3 (13.5 ± 0.48)

[a] Ten devices fabricated from the same batch and the average performance is shown in parentheses.

shown in Fig. 2 and summarized in Table 2. The PCE of the PSC with the dopant-free PTZ-TPA was 14.3%, with a short circuit photocurrent density (J_{sc}) of 21.5 mA cm^{-2}, an open circuit voltage (V_{oc}) of 0.982 V, and a fill factor (FF) of 0.679. As shown in Fig. S6,† the stabilized power outputs were 14.00% for the PTZ-TPA-based devices, which is consistent with the obtained PCEs. Under the same fabrication conditions, the best devices based on pristine Spiro-MeOTAD showed a dramatic decrease of the J_{sc} and FF, resulted in a considerably lower PCE of merely 7.39%, which could be caused largely by the lower hole mobility of pristine Spiro-MeOTAD compared with that of PTZ-TPA. The cell based on doped Spiro-MeOTAD achieved a PCE of 17.1% with a J_{sc} of 22.5 mA cm^{-2}, a V_{oc} of 1.03 V, and a FF of 0.736. The slightly higher current using Spiro-MeOTAD can be attributed to its higher HOMO level compared with that of PTZ-TPA, which gives Spiro-MeOTAD a higher driving force for charge transfer from the perovskite to the HTM layer. The lower J_{sc} values obtained for devices based on PTZ-TPA compared with for doped Spiro-MeOTAD is in agreement with the IPCE spectra shown in Fig. 2b. The device that contained Spiro-MeOTAD exhibited a much higher FF, resulting in a significantly increased PCE. The devices with PTZ-TPA showed a slightly lower open circuit voltage (V_{oc} = 0.982 V) than the devices employing Spiro-MeOTAD (V_{oc} = 1.03 V). However, our ionization energy measurement system data show that the HOMO energy level of PTZ-TPA is deeper than that of Spiro-MeOTAD, which should result in a higher V_{oc}. As the V_{oc} depends on (1) the splitting of the Fermi levels for the photogenerated charges, (2) the recombination dynamics, and (3) the energetics of the devices,[33–35] the slightly lower voltage in the devices fabricated with PTZ-TPA as the HTM might be caused by a higher recombination rate. This would suggest that PTZ-TPA has slightly inferior charge extraction capabilities compared with Spiro-MeOTAD. The statistics for the device characteristics (V_{oc}, J_{sc}, FF, and PCE) collected from the same batch are presented in Fig. 3; the data demonstrate the good reproducibility of PSCs employing PTZ-TPA as a HTM.

To further understand the origin of the low V_{oc} obtained of the PTZ-TPA devices, the charge-carrier dynamics at the

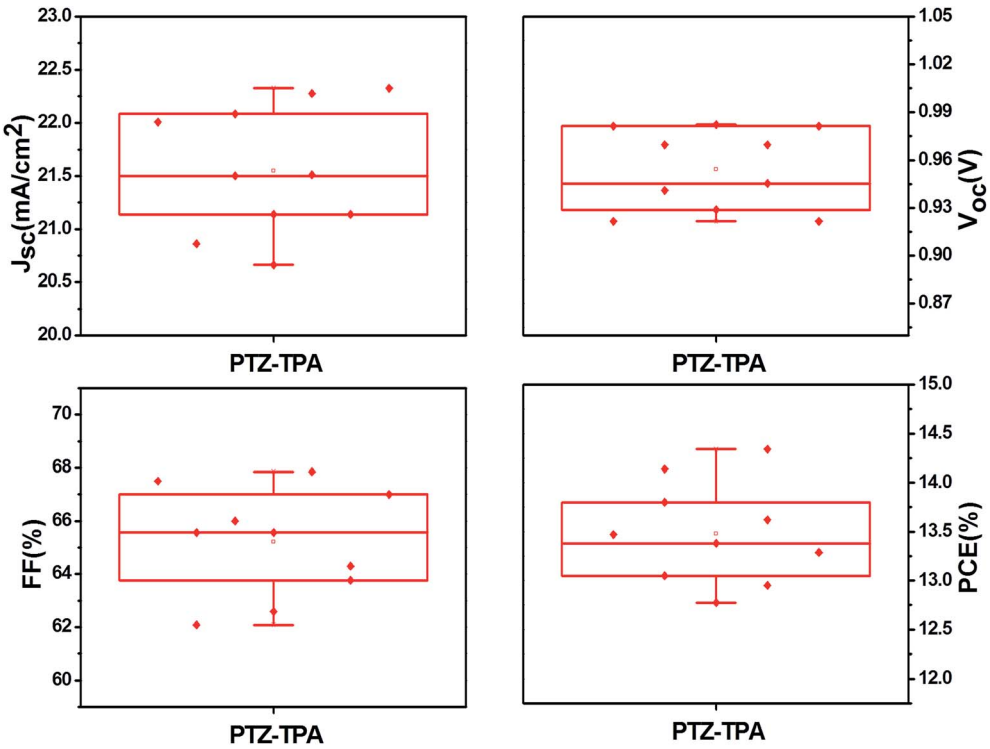

Fig. 3 Statistical data of the photovoltaic parameters for devices containing PTZ-TPA; all data points were collected from the same batch of devices.

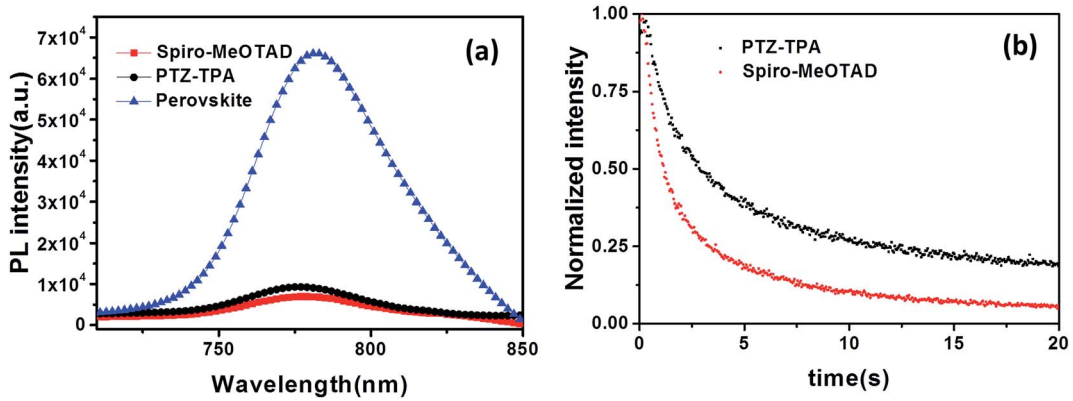

Fig. 4 (a) Steady state photoluminescence (PL) spectra of a perovskite film (blue line), a perovskite film with Spiro-MeOTAD (red line), and a perovskite film with a PTZ-TPA (black line) quenching layer; (b) normalized time-resolved photoluminescence spectra of a glass/perovskite/PTZ-TPA sample (black line) and a glass/perovskite/Spiro-MeOTAD sample (red line).

perovskite/HTM interface and hole extraction ability were investigated using steady-state and time-resolved PL (TRPL) measurements; in such measurements efficient quenching of the steady-state PL and a reduction of the PL lifetime would indicate efficient charge extraction at the perovskite/HTM interface. From the PL spectra (Fig. 4a), it is evident that both HTMs significantly quench the perovskite emission signal, with HTM Spiro-MeOTAD having a slightly better PL quenching efficiency compared with PTZ-TPA. The time-resolved PL measurements were conducted with an excitation wavelength of 405 nm and the response was monitored across the entire emission spectral range (Fig. 4b). The $CH_3NH_3PbI_3$/Spiro-MeOTAD samples showed a decay time of 0.7655 ns, whereas the $CH_3NH_3PbI_3$/PTZ-TPA samples showed a longer decay lifetime of 1.250 ns. This indicates that Spiro-MeOTAD has a slightly better hole extraction ability than PTZ-TPA. As a result, it is unlikely that further device optimization will enable the device performance of PTZ-TPA to exceed that of Spiro-MeOTAD-based devices. Thus, the much lower cost of PTZ-TPA, owing to its simpler synthesis methods, in combination with its comparable device performance might offer a potentially lower cost/power ratio, which is the ultimate economic criterion for photovoltaic systems.

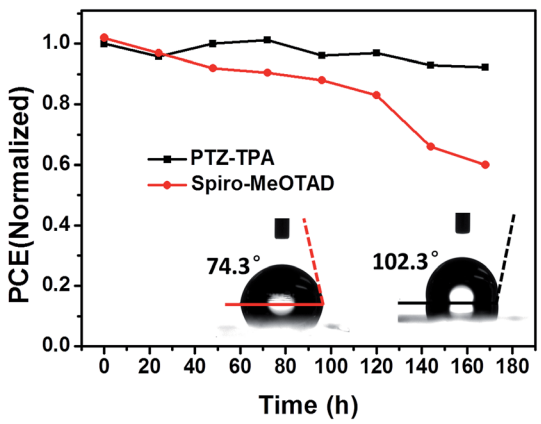

Fig. 5 Normalized PCEs of PSCs as a function of time. After each J–V measurement, the device was removed from the applied light illumination and stored in ambient air without encapsulation. The humidity of the atmosphere was about 30%. The inset shows the water contact angles of thin films of pristine PTZ-TPA (102.3°) and of Spiro-MeOTAD (74.3°) doped with Li-TFSI and TBP.

To further demonstrate the improvements using PTZ-TPA yielded for PSCs, we investigated the long-term stability of devices using these HTMs; we performed stability tests of PSCs without encapsulation and under identical storage conditions (storage time = 168 h). As seen in Fig. 5, the PCEs of PSCs with Spiro-MeOTAD (doped) as the HTM retained only 59% of their initial efficiency. However, the PTZ-TPA-based devices exhibited a PCE retention of 92%. This result clearly demonstrates the excellent device stability of PSCs with PTZ-TPA HTMs over the course of a week. As reported by many research groups, higher stabilities are recorded for PSCs with a hydrophobic HTM; the greater the hydrophobicity, the higher the stability.[36] The PTZ-TPA film (Fig. 5) shows a larger water contact angle of 102.3° than Spiro-MeOTAD (74.3°), which effectively prevents moisture penetration into the perovskite layer. PTZ-TPA has a sufficient number of alkyl chains to be solution processable. Furthermore, alkyl chains improve hydrophobicity, which in turn improves the stability of the resulting PSCs.[26,36]

4. Conclusions

In conclusion, a HTM PTZ-TPA-based phenothiazine core was designed and prepared using a simple one-step synthesis procedure using inexpensive commercial precursors with a high yield. We employed the new material as a hole transporting layer in $CH_3NH_3PbI_3$-based perovskite solar cells. With the PTZ-TPA HTM without dopants a PCE of 14.3% was achieved, which is comparable to that of devices based on the well-known doped HTM Spiro-MeOTAD (17.1%). Long-term stability studies showed that the PTZ-TPA-based devices were more stable when exposed to air than cells employing Spiro-MeOTAD. The low-cost, facile one-step synthetic method as well as the excellent hole mobility and appropriate energy level makes PTZ-TPA a promising

candidate to substitute Spiro-MeOTAD in the large scale production of high performance, stable perovskite solar cells.

Conflicts of interest

There are no conflicts to declare.

Acknowledgements

The work at South University of Science and Technology of China was supported by Special Funds for the Development of Strategic Emerging Industries in Shenzhen (JCYJ20170412154240645). This research was also supported by the National Basic Research Program of China (Fundamental Studies of Perovskite Solar Cells 2015CB932200), and National Natural Science Foundation of China (Nos. 51373076, 91433118, 61605075).

References

1 M. M. Lee, J. Teuscher, T. Miyasaka, T. N. Murakami and H. J. Snaith, *Science*, 2012, **338**, 643–647.
2 H.-S. Kim, C.-R. Lee, J.-H. Im, K.-B. Lee, T. Moehl, A. Marchioro, S.-J. Moon, R. Humphry-Baker, J.-H. Yum, J. E. Moser, M. Grätzel and N.-G. Park, *Sci. Rep.*, 2012, **2**, 591.
3 W. Chen, Y. Wu, Y. Yue, J. Liu, W. Zhang, X. Yang, H. Chen, E. Bi, I. Ashraful, M. Grätzel and L. Han, *Science*, 2015, **350**, 944–948.
4 F. Bella, G. Griffini, J.-P. Correa-Baena, G. Saracco, M. Grätzel, A. Hagfeldt, S. Turri and C. Gerbaldi, *Science*, 2016, aah4046.
5 A. Kojima, K. Teshima, Y. Shirai and T. Miyasaka, *J. Am. Chem. Soc.*, 2009, **131**, 6050–6051.
6 W. S. Yang, B.-W. Park, E. H. Jung, N. J. Jeon, Y. C. Kim, D. U. Lee, S. S. Shin, J. Seo, E. K. Kim, J. H. Noh and S. I. Seok, *Science*, 2017, **356**, 1376–1379.
7 Z. Yu and L. Sun, *Adv. Energy Mater.*, 2015, **5**, 1500213.
8 S. Ameen, M. A. Rub, S. A. Kosa, K. A. Alamry, M. S. Akhtar, H.-S. Shin, H.-K. Seo, A. M. Asiri and M. K. Nazeeruddin, *ChemSusChem*, 2016, **9**, 10–27.
9 J. Liu, Y. Wu, C. Qin, X. Yang, T. Yasuda, A. Islam, K. Zhang, W. Peng, W. Chen and L. Han, *Energy Environ. Sci.*, 2014, **7**, 2963.
10 Y. Liu, Q. Chen, H.-S. Duan, H. Zhou, Y. Yang, H. Chen, S. Luo, T.-B. Song, L. Dou, Z. Hong and Y. Yang, *J. Mater. Chem. A*, 2015, **3**, 11940–11947.
11 Y.-K. Wang, Z.-C. Yuan, G.-Z. Shi, Y.-X. Li, Q. Li, F. Hui, B.-Q. Sun, Z.-Q. Jiang and L.-S. Liao, *Adv. Funct. Mater.*, 2016, **26**, 1375–1381.
12 J. Zhang, B. Xu, L. Yang, A. Mingorance, C. Ruan, Y. Hua, L. Wang, N. Vlachopoulos, M. Lira-Cantú, G. Boschloo, A. Hagfeldt, L. Sun and E. M. J. Johansson, *Adv. Eng. Mater.*, 2017, **7**, 1602736.
13 Y. Liu, Z. Hong, Q. Chen, H. Chen, W.-H. Chang, Y. Yang, T.-B. Song and Y. Yang, *Adv. Mater.*, 2016, **28**, 440–446.
14 S. Jeon, U. K. Thakur, D. Lee, W. Yin, D. Kim, S. Lee, T. K. Ahn, H. J. Park and B. G. Kim, *Org. Electron.*, 2016, **37**, 134–140.
15 F. Zhang, C. Yi, P. Wei, X. Bi, J. Luo, G. Jacopin, S. Wang, X. Li, Y. Xiao, S. M. Zakeeruddin and M. Grätzel, *Adv. Eng. Mater.*, 2016, **6**, 1600401.
16 F. Zhang, X. Zhao, C. Yi, D. Bi, X. Bi, P. Wei, X. Liu, S. Wang, X. Li, S. M. Zakeeruddin and M. Grätzel, *Dyes Pigm.*, 2017, **136**, 273–277.
17 G.-W. Kim, G. Kang, J. Kim, G.-Y. Lee, H. I. Kim, L. Pyeon, J. Lee and T. Park, *Energy Environ. Sci.*, 2016, **9**, 2326–2333.
18 F. Wu, B. Wang, R. Wang, Y. Shan, D. Liu, K. Y. Wong, T. Chen and L. Zhu, *RSC Adv.*, 2016, **6**, 69365–69369.
19 C. Huang, W. Fu, C.-Z. Li, Z. Zhang, W. Qiu, M. Shi, P. Heremans, A. K. Y. Jen and H. Chen, *J. Am. Chem. Soc.*, 2016, **138**, 2528–2531.
20 G. Gong, N. Zhao, D. Ni, J. Chen, Y. Shen, M. Wang and G. Tu, *J. Mater. Chem. A*, 2016, **4**, 3661–3666.
21 X. Liu, X. Zheng, Y. Wang, Z. Chen, F. Yao, Q. Zhang, G. Fang, Z.-K. Chen, W. Huang and Z.-X. Xu, *ChemSusChem*, 2017, **10**, 2833.
22 G. Yang, Y.-L. Wang, J.-J. Xu, H.-W. Lei, C. Chen, H.-Q. Shan, X.-Y. Liu, Z.-X. Xu and G.-J. Fang, *Nano Energy*, 2017, **31**, 322–330.
23 M. Cheng, X. Yang, C. Chen, Q. Tan and L. Sun, *J. Mater. Chem. A*, 2014, **2**, 10465–10469.
24 M. Cheng, B. Xu, C. Chen, X. Yang, F. Zhang, Q. Tan, Y. Hua, L. Kloo and L. Sun, *Adv. Energy Mater.*, 2015, **5**, 1401720.
25 M. Cheng, C. Chen, X. Yang, J. Huang, F. Zhang, B. Xu and L. Sun, *Chem. Mater.*, 2015, **27**, 1808–1814.
26 Y. Wang, X. Liu, H. Shan, Q. Chen, T. Liu, X. Sun, D. Ma, Z. Zhang, J. Xu and Z.-X. Xu, *Dyes Pigm.*, 2017, **139**, 619–626.
27 R. Grisorio, B. Roose, S. Colella, A. Listorti, G. P. Suranna and A. Abate, *ACS Energy Lett.*, 2017, **2**, 1029–1034.
28 Y. Hou, H. Zhang, W. Chen, S. Chen, C. O. R. Quiroz, H. Azimi, A. Osvet, G. J. Matt, E. Zeira, J. Seuring, N. Kausch-Busies, W. Lövenich and C. J. Brabec, *Adv. Energy Mater.*, 2015, **5**, 1500543.
29 Y. Sun, G. C. Welch, W. L. Leong, C. J. Takacs, G. C. Bazan and A. J. Heeger, *Nat. Mater.*, 2012, **11**, 44.
30 W. Ke, G. Fang, Q. Liu, L. Xiong, P. Qin, H. Tao, J. Wang, H. Lei, B. Li, J. Wan, G. Yang and Y. Yan, *J. Am. Chem. Soc.*, 2015, **137**, 6730–6733.
31 C. Teng, X. Yang, C. Yang, S. Li, M. Cheng, A. Hagfeldt and L. Sun, *J. Phys. Chem. C*, 2010, **114**, 9101–9110.
32 A. Krishna, D. Sabba, J. Yin, A. Bruno, L. J. Antila, C. Soci, S. Mhaisalkar and A. C. Grimsdale, *J. Mater. Chem. A*, 2016, **4**, 8750–8754.
33 N. J. Jeon, J. Lee, J. H. Noh, M. K. Nazeeruddin, M. Grätzel and S. I. Seok, *J. Am. Chem. Soc.*, 2013, **135**, 19087–19090.
34 A. Krishna, D. Sabba, H. Li, J. Yin, P. P. Boix, C. Soci, S. G. Mhaisalkar and A. C. Grimsdale, *Chem. Sci.*, 2014, **5**, 2702–2709.
35 A. Krishna, D. Sabba, J. Yin, A. Bruno, P. P. Boix, Y. Gao, H. A. Dewi, G. G. Gurzadyan, C. Soci, S. G. Mhaisalkar and A. C. Grimsdale, *Chem.–Eur. J.*, 2015, **21**, 15113–15117.
36 S. S. Reddy, K. Gunasekar, J. H. Heo, S. H. Im, C. S. Kim, D.-H. Kim, J. H. Moon, J. Y. Lee, M. Song and S.-H. Jin, *Adv. Mater.*, 2016, **28**, 686–693.

